Single Si dopants in GaAs studied by scanning tunneling microscopy and spectroscopy

A. P. Wijnheijmer,[1,*] J. K. Garleff,[1] K. Teichmann,[2] M. Wenderoth,[2] S. Loth,[2,3] and P. M. Koenraad[1]

[1]*COBRA Inter-University Research Institute, Department of Applied Physics, Eindhoven University of Technology, P. O. Box 513, NL-5600 MB Eindhoven, The Netherlands*

[2]*IV. Physikalisches Institut, Universität Göttingen, F.-Hund-Platz 1, D-37077 Göttingen, Germany*

[3]*IBM Research Division, Almaden Research Center, San Jose, California 95120, USA*

(Received 9 June 2011; revised manuscript received 8 August 2011; published 12 September 2011)

We present a comprehensive scanning tunneling microscopy and spectroscopy study of individual Si dopants in GaAs. We explain all the spectroscopic peaks and their voltage dependence in the band gap and in the conduction band. We observe both the filled and empty donor state. Donors close to the surface, which have an enhanced binding energy, show a second ionization ring, corresponding to the negatively charged donor D^-. The observation of all predicted features at the expected spectral position and with the expected voltage-distance dependence confirms their correct identification and the semiquantitative analyses of their energetic positions.

DOI: 10.1103/PhysRevB.84.125310 PACS number(s): 73.20.At, 68.37.Ef, 73.20.Hb

I. INTRODUCTION

It is impossible to imagine life today without semiconductors. Almost every piece of electronic equipment contains a computer chip, composed of semiconductor material. The functionality of the components on the computer chips, e.g., transistors, is realized by adding dopant atoms into the semiconductor host in order to introduce free charge carriers. Over the past few decades, the device dimensions have decreased tremendously, as was predicted by Moore in 1965.[1] Where the channel width of a transistor back in the 1980s was more than 1 μm, its width in state-of-the-art devices today is only 32 nm.[2] The random and discrete nature of dopant atoms becomes apparent at these small scales, leading to statistical variability in, e.g., the threshold voltage of the device. Current device simulations therefore take the discrete nature into account.[3–5] Research devices that are even smaller than commercial devices have reached a limit where single impurities can dominate the transport properties and where interfaces affect the properties of impurities.[6–10] Therefore, fundamental research on the atomic scale of the properties of individual dopants, interactions between neighboring dopants and the influence of interfaces and surfaces, is of crucial importance.

Scanning tunneling microscopy (STM) and spectroscopy (STS) are ideal techniques to study properties of dopants on the atomic scale. Donors in GaAs have been studied for many years by various groups[11–19] and Si:GaAs is considered a model system for a hydrogenic donor in a semiconductor.

Recently we have studied the STM-tip-induced ionization process and showed that we can ionize single silicon donors in GaAs and visualize the ionization process.[20,21] Others have shown similar results for manganese in InAs.[22] The electrostatic potential of the tip is used to ionize the individual defects. The ionization is visible in the STM and STS images as bright disks or rings, respectively, which we call ionization rings. Previously, we investigated the dependence on the sample voltage and tip-sample distance and were able to measure the Coulomb potential of a single ionized donor.[20] Furthermore we used the voltage threshold of the ionization rings to measure the binding energy of the donors as a function of depth below the surface and found a significant enhancement in contrast to the predicted reduction.[21] In this paper, we discuss these STM and STS measurements in more detail. We explain all spectroscopic features visible in the STS data. We analyze the ionization process of individual donors and observe the filled- and empty-state wave functions. The measurements reveal that a second electron can be bound to the donor and show the influence of the tip shape on the ring shape and the Coulomb interaction between neighboring donors.

II. EXPERIMENTAL

For our measurements we use an Omicron LT-STM and a home-built LT-STM, both operated at 5 K with a base pressure of $<10^{-11}$ mbar. We use Si-doped GaAs wafers with a doping concentration of $\sim 2 \times 10^{18}$ cm^{-3}. We cleave the samples in ultrahigh vacuum (UHV) to obtain a clean and atomically flat surface, which stays clean for several weeks at low temperatures. We use tungsten tips, which are electrochemically etched from polycrystalline tungsten wire. Our tips are ultra sharp; the radius is only a few nanometers.[20] Preparation in UHV, such as argon bombardment, creates tips that are stable for days to weeks at low temperature.

III. RESULTS AND DISCUSSION

Figure 1 shows a typical STM topography image of Si:GaAs{110} at a relatively low positive sample voltage of 1.25 V and 20 pA. The thin vertical lines correspond to the atomic rows. There are several bright and dark features, and some of the bright features have a disk shape. All the bright features correspond to Si donors; the donors close to the surface have a ionization disk that is very well visible, and the disk for deeper donors is less visible or not visible at all for the very deep donors. The dark contrasts are Si atoms on an arsenic site, which act as acceptors and are expected to be present in samples with a doping concentration of $>10^{18}$ cm^{-3}.[15–17,23] Donors *in* the surface layer show a bistable behavior between the normal hydrogenic donor configuration and a negatively charged configuration.[24] This bistability occurs only in topography images for $0\,\text{V} \leqslant V \leqslant 1\,\text{V}$ and is not discussed here.

 ©2011 American Physical Society

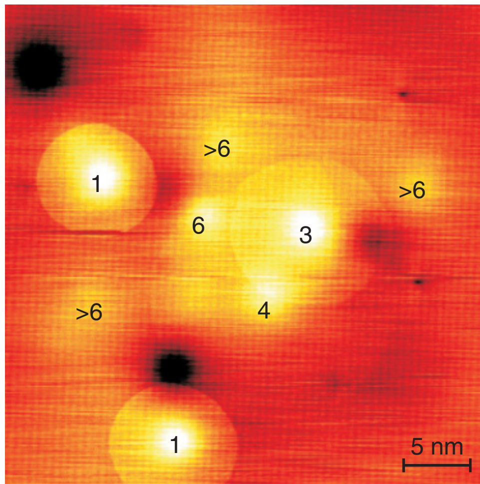

FIG. 1. (Color online) Typical STM topography image of Si-GaAs{110} at 1.25 V and 20 pA. The bright features with and without rings are Si donors, and the depth below the surface in monolayers is indicated, counting the surface layer as 1.

The topography image in Fig. 1 shows several ionization disks, belonging to donors in different depths below the surface. The ionization mechanism is explained in Ref. 20 and we give only a short summary here (see Fig. 2). When the tip is far away from the donor, it will be neutral (D^0) because the thermal energy is smaller than the binding energy at 5 K [Figs. 2(a) and 2(b)]. Due to the unpinned Fermi level of GaAs{110}, the bands are locally bent by the charged tip. The donors can be ionized by this local tip-induced band bending (TIBB),[25] which has an extension of only a few nanometers laterally and into the bulk due to the small apex radius of our tips. The TIBB is schematically depicted by the colored cloud in Figs. 2(a) and 2(c). The TIBB is upward at positive sample voltages (depletion of charge carriers), and the donor ionizes when the donor level is pushed above the Fermi level in the sample ($E_{F,s}$); see Figs. 2(c) and 2(d). The additional Coulomb potential of the positively charged donor (D^+) lowers the bands locally, and thus more states are available for tunneling when the donor is ionized ([Fig. 2(e)]. In constant current topography mode this results in a retraction of the tip, visible as the disks surrounding the donors. The donor is thus neutral outside the disk and positively ionized inside the disk.

The disks belonging to donors close to the surface are small and well visible, and the disks belonging to donors deeper below the surface are bigger and less clear. The step height at the edge of the ring reflects the Coulomb potential of the ionized donor; see Ref. 20. Consequently, the contrast is bigger for donors closer to the surface. The diameter of the disks reflects the binding energy of the donors; a small disk corresponds to a large TIBB and thus a high binding energy. Previously we showed that the binding energy is enhanced for donors close to the surface,[21] which manifests itself by the smaller disk diameter for donors close to the surface. Both effects are schematically shown in Fig. 2(f).

We performed STS on the same area of the sample as shown in Fig. 1. On a grid of 256 × 256 pixels, we took $I(V)$ spectra. We obtain the differential conductance dI/dV by numerically differentiating the $I(V)$ curves after the actual measurement.

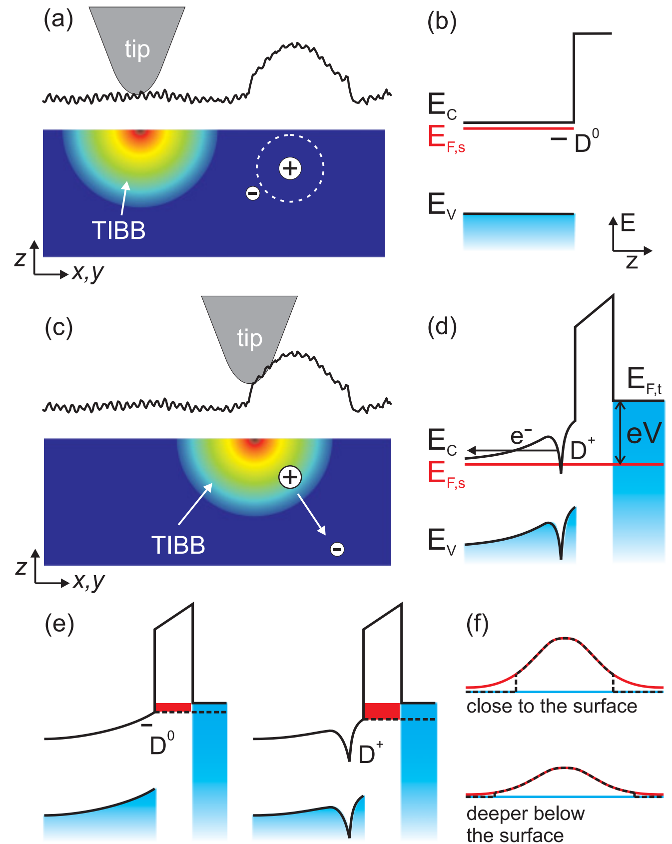

FIG. 2. (Color online) Schematic of the model of the ionization process. [(a)–(d)] The donors are ionized by the TIBB. The conduction and valence band maxima are indicated by E_C and E_V, respectively, and the Fermi level of the tip by $E_{F,t}$. The other symbols are defined in the main text. (e) The density of states available for tunneling increases due to the ionization. (f) Donors close the the surface have small disks that are well visible and deeply buried donors have bigger and less-clear disks.

The differential conductance corresponds to the local density of states (LDOS) when a constant tip-sample distance (z_t) is assumed $dI/dV \propto \text{LDOS} \times \exp(-2\kappa z_t)$. Here $\kappa \sim 1$ Å^{-1} is the inverse decay length in the vacuum. We thus obtain the LDOS as a function of x, y, and V. Typically, we use 200 to 300 voltage steps between −1.5 V and +1.0 V. The resolution after applying a Gaussian filter in the voltage direction is ∼100 mV. Several lateral dI/dV images at the indicated voltages are shown in Fig. 3. Below ∼−1.1 V Friedel-like oscillations are detected.[12] In the band gap between −1.1 V and 0.2 V, the various donors appear at different voltages and show an increasing ring diameter with voltage. They disappear when the extension has reached a few nanometers and appear again at the onset of tunneling into the conduction band (CB) at ∼0.2 V.

We discuss all these features using cross sections through the dI/dV data set. Figures 4(b)–4(d) show three dI/dV cross sections taken on top of the donors marked by Si_b-Si_d in Fig. 3. The left-hand side ($r = 0$ nm) is on top of the donor and r is the distance to the donor center. We applied an azimuthal average. The color scale represents dI/dV. We subtracted a spectrum obtained on the bare GaAs surface in order to suppress the

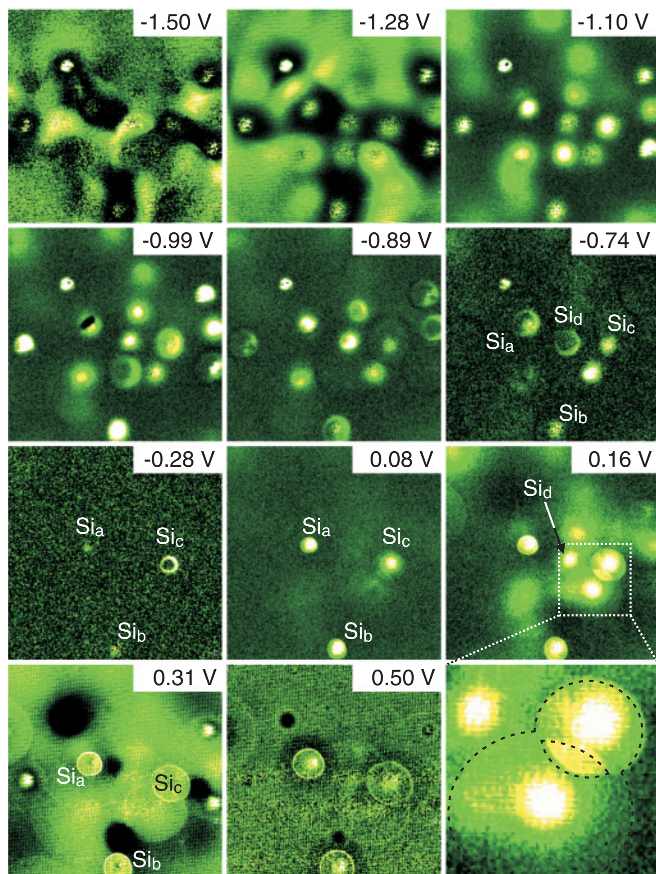

FIG. 3. (Color online) A series of spatially resolved dI/dV images at the indicated voltages. The images are 40 × 40 nm and the set point is 1.5 V and 3.15 nA.

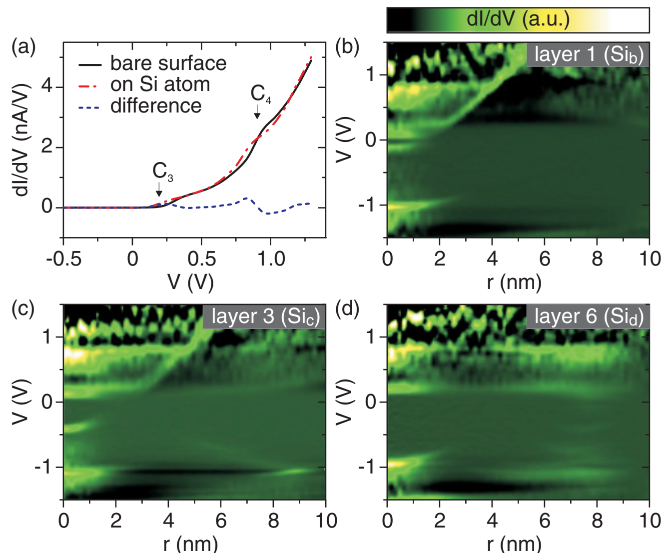

FIG. 4. (Color online) (a) Typical dI/dV curve on the bare surface (solid black) and on a Si donor (dash-dotted red) and the difference between the two (dashed blue). [(b)–(d)] Sections through the dI/dV data set on top of the donors marked Si_b-Si_d in Fig. 3, where an azimuthal average is applied. The left-hand side ($r = 0$ nm) is on top of the donor's center A spectrum on the bare surface is subtracted in order to suppress the bands.

signal from tunneling into the conduction and valence band (VB). Therefore, there is no significant signal in the images far away from the donor ($r \approx 10$ nm). Closer to the donor center, several features are visible. These features are highlighted, color coded, and numbered in Fig. 5 and explained in the next paragraphs.

One of the most striking features is the hyperbolic signature of the ring of ionization (red, 1), whose diameter increases with voltage. The donor ionizes when its level is aligned with the Fermi level in the sample, and therefore the ionization ring follows a TIBB contour. The dependence of the ring diameter on the applied voltage is qualitatively easily understood. At a higher voltage the TIBB is larger with regard to both the amount of TIBB and the extension. In other words, the colored cloud in Fig. 2 is bigger, thus the donor already ionizes when the tip is still further away from the donor. As a next step, we calculate the TIBB in three dimensions quantitatively,[20,21,25] for which we use the code developed by Feenstra.[25] It is a self-consistent Poisson solver for a hyperbolic tip near a semiconductor surface. There are several input parameters. Some are well known, such as the (average) doping concentration, temperature, band gap, and the dielectric constant. Others have to be estimated: tip shape (radius of curvature at the tip apex and the opening angle of the shank), tip-sample distance, and flat band condition. By varying these parameters within realistic limits, we can obtain perfect agreement between theory and experiment. However, the fit is not unique. We test this by varying the parameters to extreme limits. A typical tip-sample distance z_t is 5 Å. The measurement shown in Fig. 3 was measured with a set point of 1.5 V and 3.15 nA, which is a higher current set point than typically used. We thus assume that 7 Å is the upper limit and as a lower limit we choose 3 Å. We calculate the TIBB for

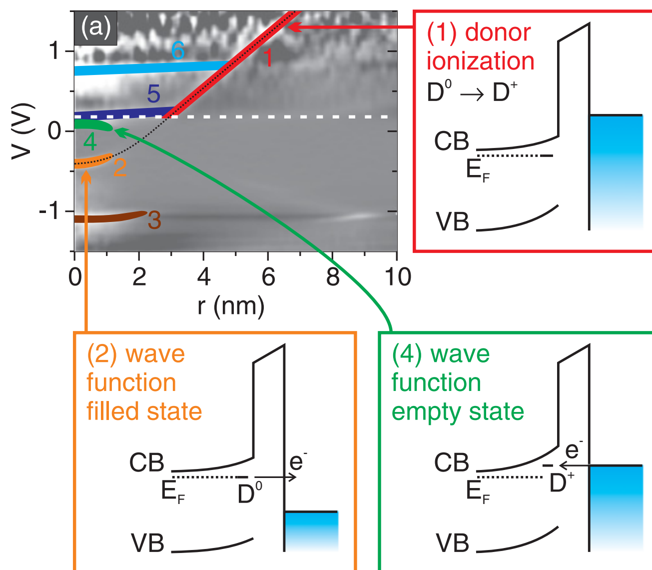

FIG. 5. (Color online) (a) All features in the section shown in Fig. 4(c) are highlighted, numbered, and color coded. Schematics of (1) the ionization process, (2) the filled-state wave function, and (4) the empty-state wave function. The black dotted line is added to guide the eye and the white dashed line marks the onset of the CB.

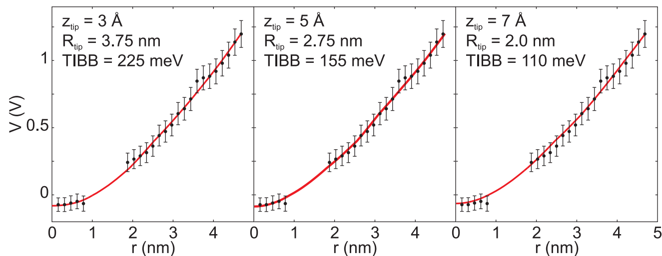

FIG. 6. (Color online) Experimentally obtained ionization curve (black dots) and calculated TIBB contour (red line) for three different parameter sets.

these three values for z_t and optimize the other parameters to fit the experimental data points.[26] The result is shown in Fig. 6. The black dots represent the experimentally observed ionization curve and the solid lines represent the calculated TIBB contours. The latter corresponds to the sample voltage that is required in order to reach the indicated TIBB value (i.e., 225 meV in the left graph of Fig. 6) at the lateral tip-donor distance r (horizontal axis). In all graphs the fit is similarly good, though the parameters differ and the total TIBB differs by a factor of 2 between the extreme cases. Even though we can only extract the TIBB with a ∼30% uncertainty, we can compare the relative values within one data set (i.e., measured with the same tip) with a much higher accuracy, as we did to measure the binding energy as a function of depth below the surface we reported earlier.[21] Choosing different TIBB parameters only adds a scaling factor to the graphs but does not affect the overall trend or the relative values.

The next feature we address is the bottom part of the hyperbolic feature (orange, 2). This contrast reflects tunneling of electrons from the filled-state donor wave function. In order to address the filled-state wave function, we have to meet two requirements. First, we have to be in the filled-state imaging mode, i.e., $V < 0$, and, second, the donor should be filled. The change from a filled to an empty donor state occurs when the donor level is aligned with the sample Fermi level.[27] Thus, the tunneling conditions for the filled-state donor wave function are the same as for the ring of ionization and the orange and red features lie on the same TIBB contour (see Fig. 6).

There is a gap between the red (1) and orange (2) feature in Fig. 5. The electron involved in the ionization does itself not contribute to the tunneling current; only the Coulomb effect is visible. Other tunneling channels are required, e.g., tunneling into the CB, in order to visualize the ionization. Therefore, the red feature appears only in the CB, and the onset of the CB is indicated by the white dashed line. The orange feature represents the wave function and therefore its extension corresponds to the projection of the Bohr radius. Figure 7 shows the normalized dI/dV intensity versus distance to the donor's center for donors in different depths below the surface, where the dI/dV intensity is integrated over a small voltage window around the peak and normalized by the amplitude at $r = 0$ nm. We observe that the extension of the wave function increases with increasing depth of the addressed donor below the surface. Note that this is the projection of the wave function and, therefore, its width does not directly correspond to the Bohr radius. Nevertheless, the smaller diameter for Si atoms closer to the surface corroborates the enhanced binding

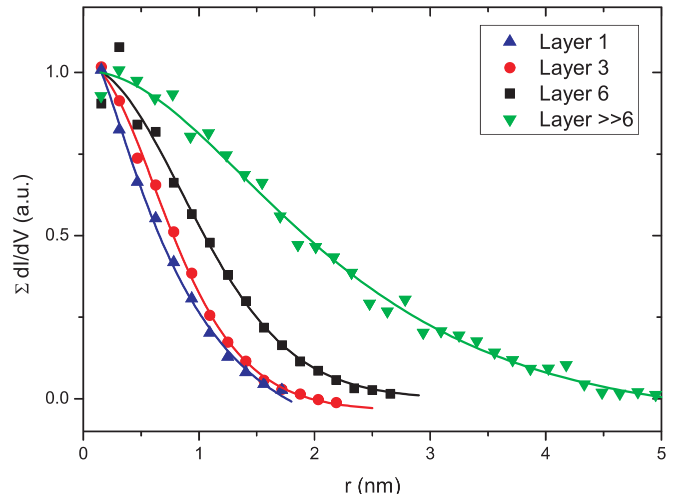

FIG. 7. (Color online) Extension of the filled-state wave function of Si donors in different depths; the dots correspond to the integrated dI/dV plotted as a function of radial distance from the dopant center and the solid lines are added to guide the eye. The extension of the filled-state wave function is larger for donors deeper below the cross-sectional surface.

energy.[21] The extension is a factor of ∼3 smaller for donors close to the surface compared to the deeply buried donors. In the particle-in-a-box approach as a first-order approach, a reduction of the Bohr radius by a factor of ∼ 3 corresponds to an enhanced binding energy of a factor of ∼9. In our recent publication we found a similar ratio: an enhancement to ∼40 meV for donors close to the surface compared to the bulk binding energy of 5 meV.

The donors in layer 1 and 3 have a sharp feature around −1 V, highlighted in brown (3) in Fig. 5. We suggest that this is the filled-state wave function for a second electron that can bind to a hydrogenic donor. For a bulk Si atom in GaAs with a binding energy of 5.6 meV, the binding energy of the second electron is only 0.3 meV (5.55% of the normal $D^0 \rightarrow D^+$ binding energy).[28] Donors close to the surface have an enhanced binding energy,[21] and, therefore, we expect that the binding energy of the second electron is enhanced as well. This second ring should follow a contour line of the TIBB with a lower value. We extracted the position of both rings for the two donors in layer 1 in Fig. 3 (labeled Si_a and Si_b). The result and the calculated TIBB is shown in Fig. 8. Both are surface donors measured within the same data set, so they should follow the same TIBB contour. We observe that they differ slightly. Moreover, the exact shape of the second ring (brown feature) differs for both donors; the second ring of Si_a is somewhat flatter than the second ring of Si_b. This is probably due to the local environment, which can change both the local TIBB (local doping concentration) and the binding energy of the donor itself. On average, we indeed see that the second ring follows a TIBB contour line with a lower value than the contour line that follows the first ring. The difference in the TIBB between the first and second ring is approximately a factor of 10, whereas a factor of 18 is expected, because the binding energy of the second electron is 5.55 % of binding energy of the first ring.[28] We can explain this difference qualitatively as follows. The TIBB contours do not directly equal the binding

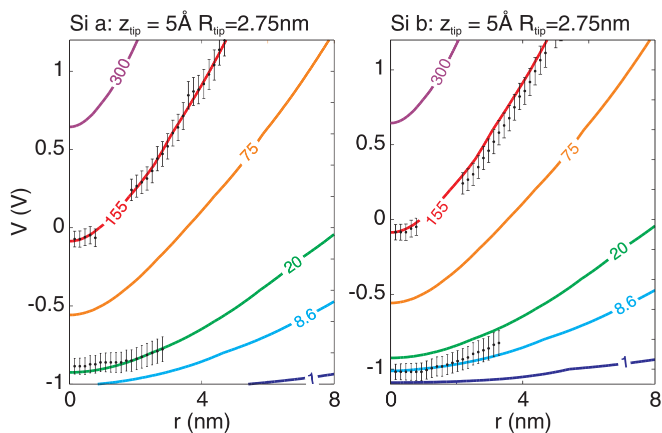

FIG. 8. (Color online) Experimentally obtained ionization curves (dots) and calculated TIBB contours in millielectron volts (lines) for two surface donors. Donors close to the surface have a second ring around −1 V.

energy as we explained in Ref. 21; see Fig. 9. The extension of the TIBB is of the same order as the width of the Coulomb potential. Therefore the donor level is not rigidly shifted with the bands. Instead, the Coulomb potential is squeezed by the TIBB, which pushes the donor level upward (thick blue line in Fig. 9). When this shift equals the binding energy, and the donor level becomes resonant with the CB, the donor ionizes. This mechanism adds a lever arm to the TIBB: A TIBB of ∼150 meV is needed in order to ionize a donor with a binding energy of ∼40 meV. This lever arm depends on the overlap between the TIBB and the wave function. We expect the wave function of the second electron to be larger than the wave function of the first electron due to its lower binding energy, which is also confirmed by our measurements. The overlap between the wave function and the TIBB is therefore smaller for the second electron, resulting in a larger lever arm, and therefore the difference between the TIBB contour and the binding energy is larger as well. This is in qualitative agreement with our observation that the ratio between the TIBB that is needed to ionize the first and the second ring is smaller than 18. Note that we observe only a second ring for donors close to the surface, which have an enhanced binding energy. For donors deeper below the surface, which have the bulk binding energy, we observe only a single ring. For bulk donors, the binding energy of the second electron is expected to be ∼0.3 meV, which is smaller than the thermal energy at 5 K of 0.43 meV.

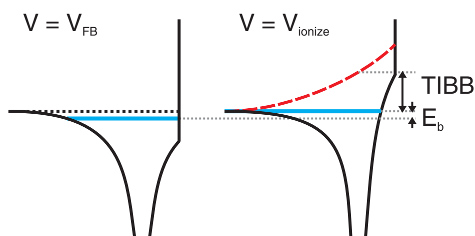

FIG. 9. (Color online) Schematic of the electrostatic potential at a donor for different sample voltages along a line perpendicular to the surface. The Coulomb potential has a similar extension as the TIBB. This adds a lever arm: a TIBB of ∼150 meV is needed in order to ionize a donor with a binding energy of ∼40 meV.

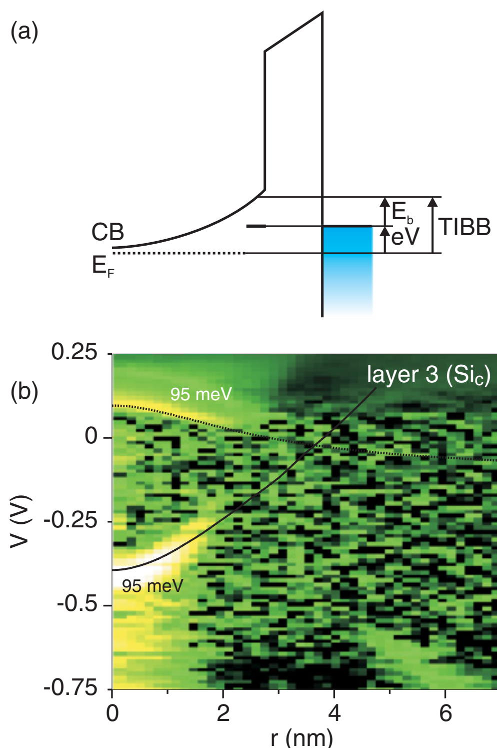

FIG. 10. (Color online) (a) Schematic of the voltage condition for tunneling into the empty-state wave function. (b) Zoom of the dI/dV section through Si_c (layer 3) with the calculated contours of the filled- and empty-state wave function.

We, therefore, do not expect to observe a second ring for deeply buried donors.

The empty-state wave function is also present in our measurements, highlighted in green (4) in Fig. 5. A zoom of this state, where we enhanced the contrast, is shown in Fig. 10(b), where the downward curvature is clearly visible. In order to address the empty-state wave function, the Fermi level of the tip has to align with the donor level. This occurs at small positive voltages and is schematically shown in Fig. 10(a). From this schematic it is clear that the voltage condition for tunneling into the empty-state wave function is

$$eV = \text{TIBB} - E^\star, \tag{1}$$

where TIBB $> E^\star$, so $eV > 0$. Experimentally we observe that the empty-state wave function appears at a lower voltage for increasing r. When the tip is laterally removed from the donor, the TIBB at the donor center is smaller, and, thus, a lower voltage is needed to align the Fermi level of the tip with the donor level [Eq. (1)]. We can calculate this voltage using the TIBB calculations[25] and assuming a certain $E^\star$. Note that this is an iterative process, as the voltage condition depends on the TIBB and the TIBB depends on the voltage. For a donor in layer 3 (Si_c), the best result is obtained for $E^\star = 95$ meV and is shown in Fig. 10(b). The TIBB contour at 95 meV is added as well, which nicely follows the filled-state wave function as expected. Note that the extra lever arm that we discussed above also holds for the empty-state wave function. The donor level does not rigidly follow the bands, and, therefore, the level as drawn in Fig. 10(a) is deeper than it would be in the rigid

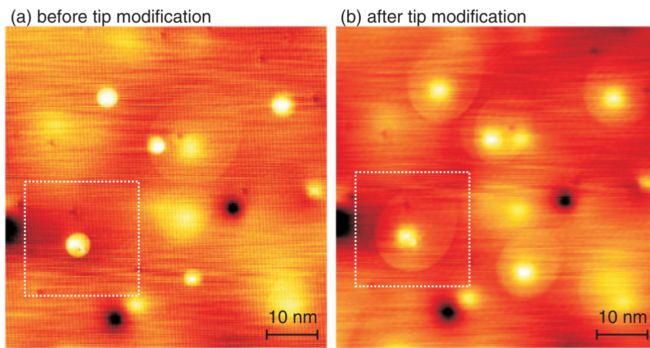

FIG. 11. (Color online) STM topographies of the same sample area (a) before and (b) after a tip modification. Both are measured at 0.6 V and 100 pA.

band model. We, therefore, find an apparent binding energy ($E^{\star} = 95$ meV) that is higher than the real binding energy E_b.

The last two features in Fig. 5 are highlighted in blue and cyan (5 and 6). We observe features around 0.2 V and 1.0 V in the spectrum obtained on the bare surface [Fig. 4(a)]. They correspond to tunneling into the C_3 and C_4 surface states.[29–31] Theoretically, these states are located 0.5 V and 1.0 V above the onset of the conduction band. Due to the Coulomb potential of the positively ionized donor, these features are shifted to lower voltages inside the ring. Subtracting a spectrum obtained on the bare surface, as we did in Figs. 4(b)–4(d), induces a peak, followed by a negative contrast, inside the ring around 0.2 V and 1.0 V.

In the results presented so far, we observe an almost perfectly circular disk or ring that is almost exactly centered around the donor. The rings in, for example, Ref. 22 show deviations from a circular ring, and the center of the ring does not coincide with the acceptor's position. The donor or acceptor contrast itself is measured by the last atom of the tip. The ring's shape and position are defined by the overall shape of the tip on a scale of several nanometers. The overall tip shape does not have to be circular symmetric and the last atom through which the tunneling current flows does not have to be located at the middle of the tip apex. The effect of the tip properties is nicely visible in Fig. 11. Both images are measured at the same location and at the same tunneling conditions. Between the measurements there was a tip modification and a few atoms dropped from the tip on the sample. This modification occurred on a different area of the sample, and, after the modification, we returned to the original area. Due to this change in the tip (the shape, the work function, or both), the disks change from almost perfect circles to egg-shaped disks.

The Coulomb interaction is also present in our measurements, visible as the reduced diameter of the rings where they overlap, see, e.g., the zoom of the dI/dV image at 0.16 V (bottom right image of Fig. 3). This effect is explained in detail in Ref. 32, and we describe only it qualitatively here. When a donor is ionized, it adds an additional attractive potential to a neighboring donor. A higher voltage is thus needed to ionize this second donor, which is visible as a reduced ring diameter. The rings are only reduced in diameter where they overlap, because the donors are neutral outside the rings and a neutral donor does not influence a neighboring donor.

IV. SUMMARY

We have performed spatially resolved scanning tunneling spectroscopy on Si-doped GaAs. Analysis of the spectra and the images lead to a comprehensive understanding of all the features in the measurements. Several observations are worth noting. We showed that we can ionize single Si donors by the STM tip, and we can visualize this ionization process. Our model reproduces the observed dependence of the ionization process on the applied voltage. The ionization rings were not observed in the early STM studies of Si:GaAs,[11–19] because much blunter tips were used, with radii of ~100 nm. In a previous publication we showed that we can extract the binding energy from the ionization threshold, and we showed that it is enhanced for donors close to the surface. This result is corroborated in the current work by the reduced extension of the wave function toward the surface and by the energetic position of the empty-state wave function. The empty-state wave function was already indentified by Feenstra *et al.*,[13] but only an approximate quantitative analysis on its energetic position was performed, and, furthermore, the voltage shift with distance to the donor center was not observed. Finally, we showed that a second electron can be bound to donors close to the surface, which is a result of their enhanced binding energies. All the analyses fit together, and this leads to a comprehensive study of STM and STS on Si-doped GaAs.

ACKNOWLEDGMENTS

We thank R. G. Ulbrich for his contributions in the early stage of this project. This work was supported by DFG-SFB 602, DFG-SPP 1285, and NAMASTE.

*a.p.wijnheijmer@tue.nl

[1] G. E. Moore, Electronics **38** (1965).
[2] *International Technology Roadmap for Semiconductors 2009 Edition*, (2009) [www.itrs.net].
[3] M. F. Bukhori, S. Roy, and A. Asenov, Microelectron. Reliab. **48**, 1549 (2008).
[4] B. Cheng, S. Roy, A. R. Brown, C. Millar, and A. Asenov, Solid-State Electron. **53**, 767 (2009).
[5] S. Roy and A. Asenov, Science **309**, 388 (2005).
[6] H. Sellier, G. P. Lansbergen, J. Caro, S. Rogge, N. Collaert, I. Ferain, M. Jurczak, and S. Biesemans, Phys. Rev. Lett. **97**, 206805 (2006).
[7] G. P. Lansbergen, R. Rahman, C. J. Wellard, I. Woo, J. Caro, N. Collaert, S. Biesemans, G. Klimeck, L. C. L. Hollenberg, and S. Rogge, Nat. Phys. **4**, 656 (2008).
[8] S. Rogge, Nat. Nano. **5**, 100 (2010).

[9]M. Pierre, R. Wacquez, X. Jehl, M. Sanquer, M. Vinet, and O. Cueto, Nat. Nano. **5**, 133 (2010).
[10]P. M. Koenraad and M. E. Flatté, Nat. Mater. **10**, 91 (2011).
[11]J. F. Zheng, X. Liu, N. Newman, E. R. Weber, D. F. Ogletree, and M. Salmeron, Phys. Rev. Lett. **72**, 1490 (1994).
[12]M. C. M. M. van der Wielen, A. J. A. van Roij, and H. van Kempen, Phys. Rev. Lett. **76**, 1075 (1996).
[13]R. M. Feenstra, G. Meyer, F. Moresco, and K. H. Rieder, Phys. Rev. B **66**, 165204 (2002).
[14]A. Depuydt, C. Van Haesendonck, N. S. Maslova, V. I. Panov, S. V. Savinov, and P. I. Arseev, Phys. Rev. B **60**, 2619 (1999).
[15]C. Domke, Ph. Ebert, M. Heinrich, and K. Urban, Phys. Rev. B **54**, 10288 (1996).
[16]C. Domke, Ph. Ebert, and K. Urban, Surf. Sci. **415**, 285 (1998).
[17]Ph. Ebert, Surf. Sci. Rep. **33**, 121 (1999).
[18]H. W. M. Salemink, M. B. Johnson, O. Albrektsen, and P. Koenraad, Solid-State Electron. **37**, 1053 (1994).
[19]M. Wenderoth *et al.*, Europhys. Lett. **45**, 579 (1999).
[20]K. Teichmann, M. Wenderoth, S. Loth, R. G. Ulbrich, J. K. Garleff, A. P. Wijnheijmer, and P. M. Koenraad, Phys. Rev. Lett. **101**, 076103 (2008).
[21]A. P. Wijnheijmer, J. K. Garleff, K. Teichmann, M. Wenderoth, S. Loth, R. G. Ulbrich, P. A. Maksym, M. Roy, and P. M. Koenraad, Phys. Rev. Lett. **102**, 166101 (2009).
[22]F. Marczinowski, J. Wiebe, F. Meier, K. Hashimoto, and R. Wiesendanger, Phys. Rev. B **77**, 115318 (2008).
[23]S. Loth, M. Wenderoth, K. Teichmann, and R. G. Ulbrich, Solid State Commun. **145**, 551 (2008).
[24]J. K. Garleff, A. P. Wijnheijmer, C. N. van den Enden, and P. M. Koenraad, Phys. Rev. B **84**, 075459 (2011).
[25]R. M. Feenstra, J. Vac. Sci. Technol. B **21**, 2080 (2003).
[26]The other parameters are full opening angle tip shank: 19°; doping concentration: 2×10^{18} cm^{-3}; and flat band condition: -1.1 V.
[27]A. P. Wijnheijmer, J. K. Garleff, M. A. van der Heijden, and P. M. Koenraad, J. Vac. Sci. Technol. B **28**, 1086 (2010).
[28]S. P. Najda, C. J. Armistead, C. Trager, and R. A. Stradling, Semicond. Sci. Technol. **4**, 439 (1989).
[29]J. R. Chelikowsky and M. L. Cohen, Solid State Commun. **29**, 267 (1979).
[30]J. R. Chelikowsky and M. L. Cohen, Phys. Rev. B **20**, 4150 (1979).
[31]R. M. Feenstra, Phys. Rev. B **50**, 4561 (1994).
[32]K. Teichmann *et al.* (submitted to Nano Letters).